

Electronic properties and surface states of CeRh₂As₂

Konrad Jerzy Kapcia^{1,*} and Andrzej Ptok^{2,†}

¹*Institute of Spintronics and Quantum Information,
Faculty of Physics, Adam Mickiewicz University in Poznań,
ul. Uniwersytetu Poznańskiego 2, PL-61614 Poznań, Poland*

²*Institute of Nuclear Physics, Polish Academy of Sciences,
ul. W.E. Radzikowskiego 152, PL-31342 Kraków, Poland*

(Dated: November 3, 2023)

Locally noncentrosymmetric CeRh₂As₂ exhibits characteristic two-phase unconventional H - T superconducting phase diagram. The transition from even- to odd-parity superconducting phase is supported by the P4/nmm crystal structure and it can be induced by the external magnetic field. Dual nature of the Ce f electrons and competition between their itinerant and localized nature can be important for its physical properties. The existing electronic band structure in this material is still under debate. Energy scale occurring in the system can be important for adequate theoretical description of its superconducting properties. In this paper, we discuss electronic band structure obtained from *ab initio* calculations. We analyze electronic surface states which can be compared with recently obtained angle-resolved photoemission spectroscopy measurement (ARPES). Additionally, we present the analyses of the hopping parameters obtained from the electronic band structure. The As-Rh layers are characterized by much more significant hopping parameters between atoms than these obtained for the Ce-Ce atoms. This suggests need of a revision of the tight binding model necessary for adequate description of the physical properties of CeRh₂As₂.

I. INTRODUCTION

Recently studied CeRh₂As₂ exhibits very rare two-phase unconventional superconductivity [1]. The magnetic field along c -axis causes the transition between two different superconducting (SC) phases. This behavior leads to characteristic H - T phase diagram for $\mathbf{H} \parallel c$ (see Fig. 1). Thermodynamic measurements uncover superconductivity below $T_{SC} = 0.37$ K, while the critical magnetic field of its high-field phase is around 14 T [1]. The observed SC phases can be tuned by the external pressure, which leads to realization of the second SC dome [2]. The ⁷⁵As nuclear magnetic resonance (NMR) studies suggest that XY-type antiferromagnetic (AFM) fluctuation occur [3]. The very early theoretical calculations of the ground state support the realization of the AFM order with the magnetic order along c in this material [4]. The experimental evidence of the AFM order in CeRh₂As₂, with the Néel temperature of $T_N \approx 0.25$ K, is based on the observation of different broadenings of the nuclear quadrupole resonance (NQR) spectrum at two crystallographically nonequivalent As sites [5]. $T_N < T_{SC}$ in ambient pressure and it can suggest a coexistence of AFM and SC orders in CeRh₂As₂. Indeed, the coexistence of AFM and low-field SC phase was reported experimentally [6]. Nevertheless, the relation between T_N and T_{SC} is still under debate. Contrary to this, there is no signature of the magnetic order in the high-field SC phase [6].

The crystal structure of CeRh₂As₂ can be discussed in the context of the Ce atoms, which locally break the inversion symmetry [Fig. 1(a)]. The experimentally inves-

tigated H - T phase diagram [schematically presented on Fig. 1(b)] exhibits occurrence regions of two SC phases. This can be associated with the even-to-odd pairing transition [1, 7]. This finding is supported also by the crystal structure, which possesses a symmetry required to stabilization of the odd-parity SC state [8]. Theoretically obtained electronic band structure exhibits complex nature with Ce f orbitals in close vicinity of the Fermi level [4]. The external magnetic field can lead to the Lifshitz transition [9], and, as consequence, to the field-driven odd-parity SC phase [8]. Additionally, the Ce f electrons and competition between their itinerant and localized part can be crucial for better exploration of the realized phase transitions between two superconducting states [10]. The strong correlation realized in the system can be a source of the observed Kondo physics [8, 11–13].

In this paper, we discuss the electronic band structure and model parameters, which can be obtained from the *ab initio* study. Recently the SC phase of CeRh₂As₂ was analyzed using several theoretical models [14–16]. Such models are based on the (intra- and inter-layer) hoppings between the locally noncentrosymmetric Ce atoms. In

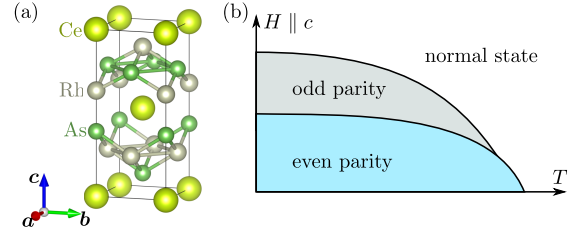


FIG. 1. (a) Crystal structure of CeRh₂As₂ and (b) its characteristic H - T phase diagram for magnetic field along c axis.

* e-mail: konrad.kapcia@amu.edu.pl

† e-mail: aptok@mmj.pl

this context, it is important to determine an energy scale of the Rashba spin-orbit coupling and the interlayer hoppings [14]. The adequate model parameters can be obtained from the *ab initio* calculations combined with the Wannier decomposition of the electronic band structure. From the other hand, the quality of the obtained electronic band structure or the Fermi surface renormalization due to the correlation effects [11] can be examined by the comparison with recently performed the angle-resolved photoemission spectroscopy (APRES) studies of CeRh_2As_2 [17, 18].

The paper is organized as follows. First, we provide the details of the computational details (Sec. II). Next, the results obtained are presented in Sec. III. In particular, we discuss the basic electronic properties of CeRh_2As_2 (Sec. III A). We also study the surface states using the tight binding model in the maximally localized Wannier orbitals, which is based on the direct calculation of the band structure (Sec. III B). Finally, we discuss the model parameters of our system (Sec. III C). A summary of the results found is presented in Sec. IV.

II. COMPUTATIONAL DETAILS

The first-principles (DFT) calculations are performed using the projector augmented-wave (PAW) potentials [19] implemented in the Vienna Ab initio Simulation Package (VASP) code [20–22]. The calculations are made within the revised Perdew–Burke–Ernzerhof for solids (PBEsol) parametrization [23], which better reproduce the experimental lattice constant [4]. The energy cut-off of the plane-wave expansion is set as 350 eV. The summation over the reciprocal space is performed with a $16 \times 16 \times 8$ Γ -centered \mathbf{k} -grid in the Monkhorst–Pack scheme [24]. The calculation includes the effects of the spin-orbit interaction. In our calculations, we use the experimental values for the lattice constants, while the atoms positions are optimized. As a break of the optimization loop, we set the energy differences to 10^{-6} eV and 10^{-8} eV for ionic and electronic degrees of freedom, respectively.

The surface states are studied by using the tight binding model in the maximally localized Wannier orbitals basis [25–27]. This model is constructed from the exact DFT calculations in a primitive unit cell, with $16 \times 16 \times 8$ \mathbf{k} -point grid, using the WANNIER90 software [28]. In the case of *f* electrons treated as a core states, we construct tight binding model based on La/Ce and Rh *d* orbitals, and As *p* orbitals, what corresponds to 42 orbitals and 84 bands in the model. Similarly, for calculation with the *f* electrons treated as a valence states, we construct model based on La/Ce *d* and *f* orbitals, Rh *d* orbitals, and As *p* orbitals, what corresponds to 56 orbitals and 112 bands in the model. The electronic surface states are calculated using the surface Green’s function technique for a semi-infinite system [29] implemented in WANNIER-TOOLS [30].

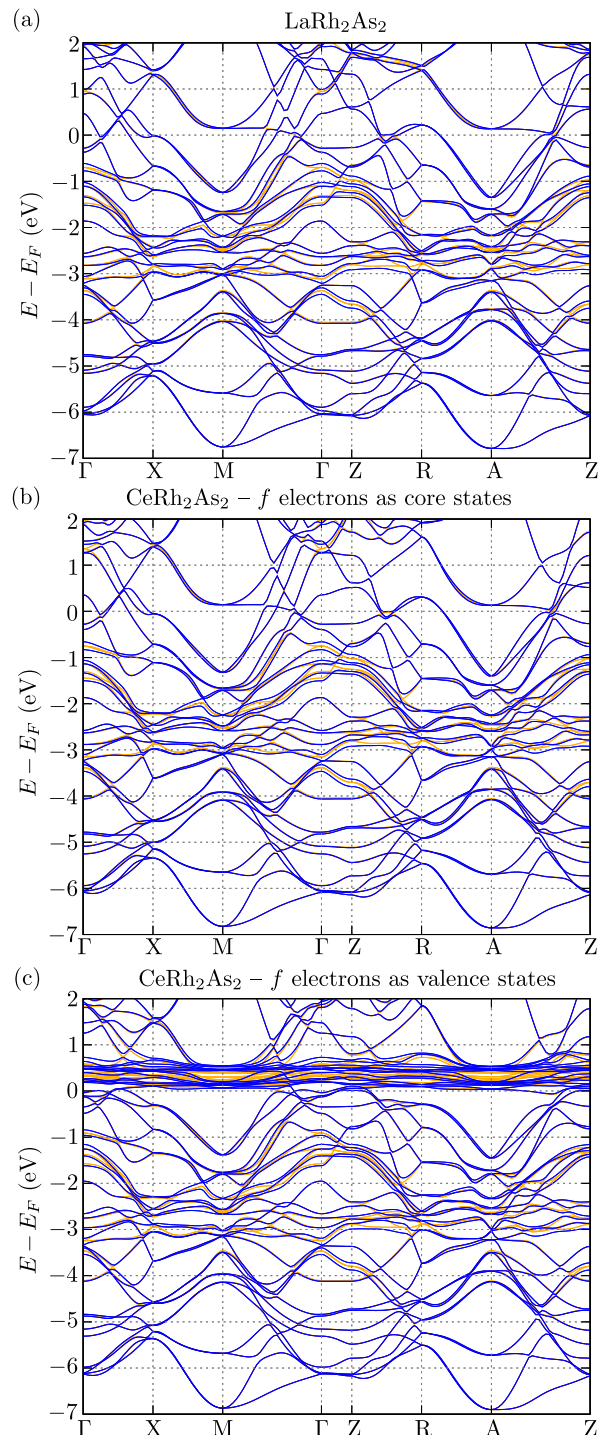


FIG. 2. Comparison of the electronic band structures of LaRh_2As_2 and CeRh_2As_2 (as labeled). In the case of CeRh_2As_2 , results for *f* electrons treated as a core states and valence states are presented (middle and bottom panel, respectively).

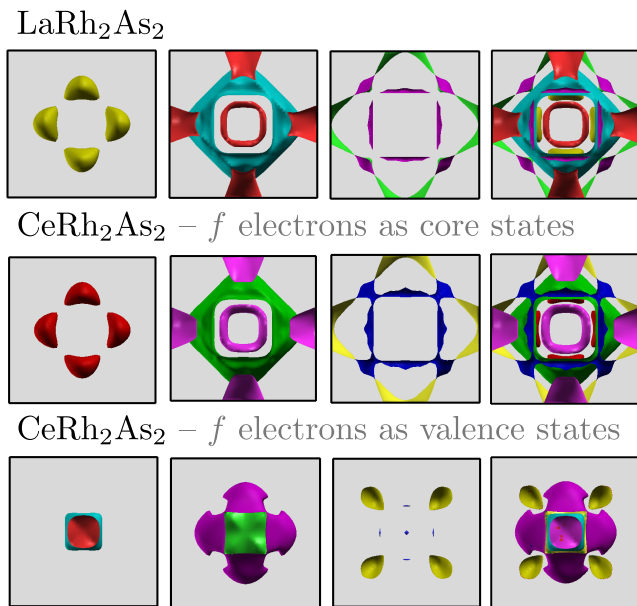


FIG. 3. Comparison of the Fermi surface (view for the top) for LaRh_2As_2 and CeRh_2As_2 (as labeled). The first two columns present the separate Fermi pockets, while the last column shows the total Fermi surface. In the case of CeRh_2As_2 , results for f electrons treated as a core states and valence states are presented (middle and bottom row, respectively).

III. RESULTS

CeRh_2As_2 compound crystallizes in the tetragonal structure with the $P4/nmm$ symmetry (space group No. 129). The experimental lattice parameters are $a = b = 4.283$ Å, and $c = 9.865$ Å [31]. The atoms are located in five non-equivalent Wyckoff positions. After optimization the atoms positions were estimated as: Ce $2c$ ($1/4, 1/4, 0.7529$), As $2a$ ($3/4, 1/4, 0$) and $2c$ ($1/4, 1/4, 0.3635$), while for Rh $2b$ ($3/4, 1/4, 1/2$) and $2c$ ($1/4, 1/4, 0.1195$). The free parameters (i.e., z -components) of atoms positions are close to this reported experimentally [1].

CeRh_2As_2 can be compared with similar material LaRh_2As_2 , which exhibits the same crystal symmetry. In this case, the experimental lattice constants are $a = b = 4.314$ Å, and $c = 9.880$ Å [31]. Similarly to the previous material, after the optimization we found atoms positions as La $2c$ ($1/4, 1/4, 0.7548$), As $2a$ ($3/4, 1/4, 0$) and $2c$ ($1/4, 1/4, 0.3644$), while for Rh $2b$ ($3/4, 1/4, 1/2$) and $2c$ ($1/4, 1/4, 0.1190$), what is comparable with the experimental values [31]. As one can see, the lattice parameters are mostly the same for both materials. Thus, LaRh_2As_2 can be treated as a reference system without f electrons around the Fermi level, what can be useful for the electronic band structure comparison and analysis.

A. Electronic band structure

The electronic properties strongly depend on the system parameters (i.e., atom positions and lattice constants). Comparison between results for LaRh_2As_2 and CeRh_2As_2 is presented in Fig. 2. In the case of CeRh_2As_2 , we present results for f electrons treated as core states [Fig. 2(b)] and as valence states [Fig. 2(c)]. In the absence of the f electrons, the electronic band structures of both compound are very similar [cf. Fig. 2(a) and Fig. 2(b)]. The f electrons are localized nearly the Fermi level [Fig. 2(c)]. After the introduction of f electrons as valence ones, an additional shift of the Fermi level is also observed [4]. These findings lead to relatively complex electronic band structure around the Fermi level, which can be simply tuned by the external magnetic field.

Mentioned sensitivity of the electronic band structure on the Fermi level is well reflected in the shape the Fermi surface (Fig. 3). In both cases of LaRh_2As_2 and CeRh_2As_2 with f electrons treated as a core state, the Fermi surfaces are very similar. Contrary to this, the Fermi surface for CeRh_2As_2 with f electrons treated as a valence states is significantly different, due to the hybridization of the d and f orbitals [4]. Additionally, any shift of the Fermi level (e.g., by doping or external magnetic field) can lead to the strong modification of the Fermi level – this effect should be strongest in the case of the 3rd Fermi pocket (see Fig. 3 – 3rd panel from the left at the bottom row). Nevertheless, realized “true” Fermi surface in CeRh_2As_2 occurring in the nature should be reflected in the ARPES results.

Here, we would like point that the Ce f states are only partially occupied. Bigger part of “flat” electronic bands with dominant f -orbital components is unoccupied. Additional effects, introduced the strong correlation on f states, typically leads to strong modification of these bands. Indeed, such effect is well visible, for example, within theoretical calculation based on the DFT+DMFT scheme [32].

B. Surface states

The analyses of the surface states starts from the slab-like calculations (Fig. 4). A realization of two layers (As-Rh-As and Rh-As-Rh) separated by Ce atoms leads to four possible terminations of the surface (left panels in Fig. 4). The electronic surface states realized on the top and the bottom surfaces (of the slab) are marked by red and blue color in Fig. 4, while bulk states are presented by grey lines. As one can expect, the surface termination strongly affect on the occurring surface states. In the case of surface terminated by Ce atoms (red lines), the well-visible surface states are realized along M-X-M path. Also along M- Γ -M path some states are visible. However, in the case of Ce-Rh termination [the top surface in Fig. 4(a)], the surface states can be realized very

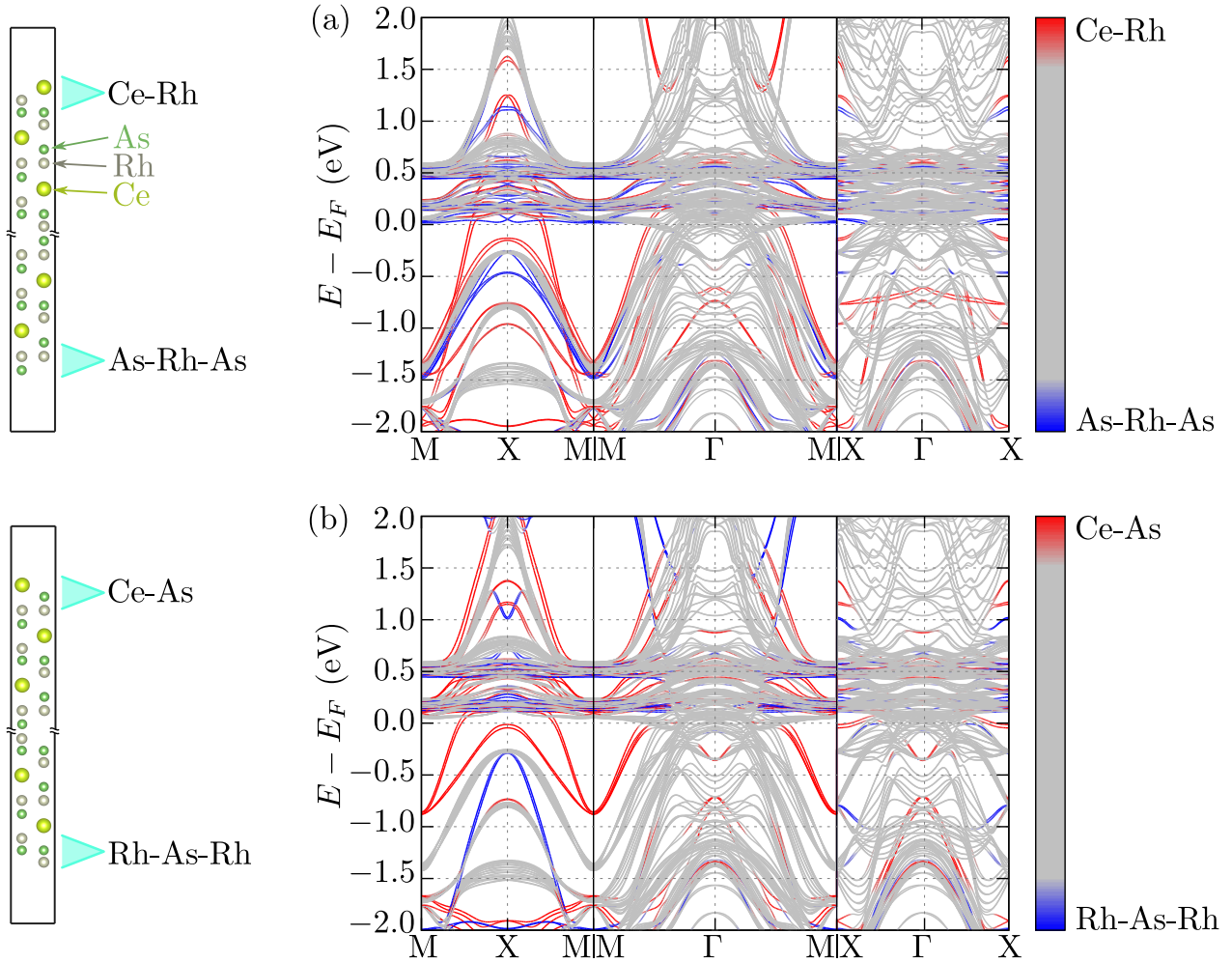


FIG. 4. The slab-like calculation for two different surface terminations (crystal structure used is presented on the left side). The first surface model contains the Ce-Rh and As-Rh-As terminations, while the second surface model includes the Ce-As and Rh-As-Rh terminations. Right panels present the electronic band structure, while color lines (red and blue) correspond to the projected band structure on the top and bottom surfaces (as presented on the left side).

closed to the bulk states. In the case of the surface terminated by As-Rh-As layer, the surface states are mostly realized above the Fermi level. This surface states are also visible along M-X-M path [blue lines in Fig. 4(a)], but close to the bulk states. The situation looks similar in the case of Rh-As-Rh layer, but in this case, the surface states along M-X-M are well-separated from the bulk states.

The difference between realized surface states is better visible in direct calculations of the surface Green's functions (Fig. 5). For simplicity and readability, we also present the spectral functions of the bulk states (the left column in Fig. 5), which for both models of the surfaces (schemata in Fig. 4) are the same. This is obvious and clear, because the bulk states do not depend by the surface termination. For all surface terminations (cf. the middle and the right column in Fig. 5), the surface states can be recognized as a separate line along M-X-M path.

Contrary to this, along M- Γ -M and X- Γ -X path, the spectrum is much more complex. Again, the f electron states are well visible above the Fermi level in the form of flat bands.

In practice, the ARPES spectra are well reproduced by our calculation. In the case of the ARPES presented in Ref. [18], we should focus on the Γ -M direction (see Fig. 2 therein). Around Γ point several hole-like bands are observed. From M to Γ point, the mostly-linear band are visible. Such bands cross the Fermi level. An absence of electron-like surface states around -0.8 eV excludes the Ce-Rh termination in this case. Also saddle point at X point is well visible, when we compare slope of the bands along X- Γ and X-M directions. This structure is also observed in the ARPES data (Fig. 3 in Ref. [18]). Contrary to the results presented in Ref. [18], we do not observe a gap at X point near the Fermi level (see Fig. 2). Realization of such a gap should not depend only on the

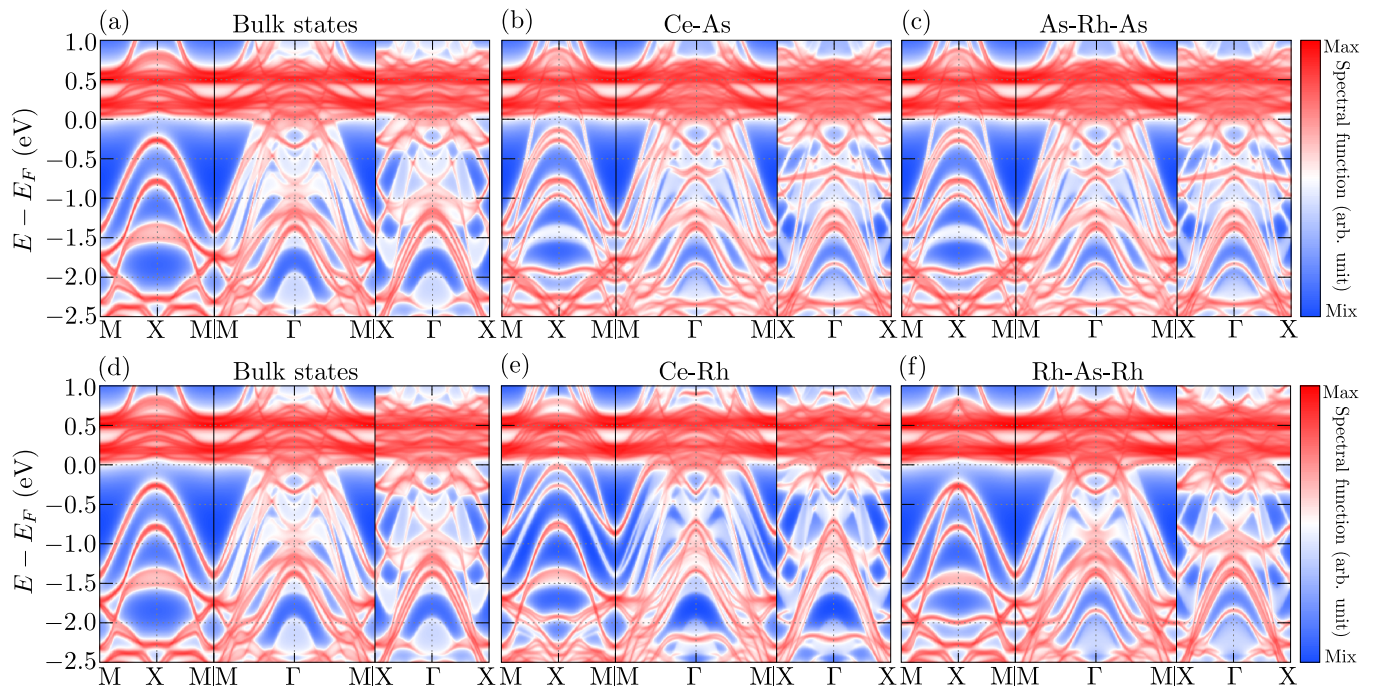


FIG. 5. Theoretically obtained spectral functions along the high-symmetry directions for the two-surface models presented in Fig. 4 (top and bottom panels, respectively). Columns from left to right correspond to bulk states, the top surface states, and the bottom surface states (as labeled).

correlations or the hybridization effect, but also on the relative distance between the energy levels of the orbitals. Similarly, the results of this work quite well agree with the ARPES experimental results presented in Ref. [17]. In this case, linear-like bands are well visible, however, the f -electron flat band is located below the Fermi level (around -0.3 eV), what suggest strong overdoping of the system in this case. Nevertheless, the band crossing observed experimentally around -1 eV is also reproduced (see Fig. 3 in Ref. [17]).

Experimentally observed ARPES spectra [17, 18], suggest that the experimentally observed Fermi level should be shifted with respect to its location obtained theoretically. Thus, the Fermi surface and constant energy contours for several energies above the Fermi level are presented on Fig. 6. The Fermi surfaces consisting of only the bulk states are presented in the first column of the figure. In the case of the theoretically obtained Fermi level, the Fermi surface from bulk states corresponds directly to those presented in Fig. 3. However, the existence of the surface states crossing the Fermi level leads to the strong modification of the predicted Fermi surface and constant energy contours for the slab-like systems (cf. the left column with other columns in Fig. 6). As we mentioned in the previous paragraph, even a small shift of the Fermi level leads to the strong modification of the results due to the complex band structure (above the Fermi level) found. Shifting the Fermi level to highest energies, the states around \bar{M} point, i.e., the around corner of the Brillouin zone, start to play stronger role (see

from top to bottom rows on Fig. 6). Moreover, the cross-like constant energy contour presented in Ref. [17] (Fig. 6 therein), suggest shifting of the Fermi level founded here by around 0.1 eV to higher energies. Nevertheless, a small difference between the constant energy contour observed experimentally and that presented in Fig. 6, suggests smaller role of correlation on the electronic band structure, which is reflected in the absence of the Fermi surface renormalization (e.g., discussed in Ref. [11]).

C. Model parameters analyses

The obtained tight binding model in the maximally localized Wannier orbital basis allow to analyze several system properties. First, the Wannier orbitals onsite energies give information about the band splitting introduced by the crystal electric field (CEF). Second, the absolute value of the hopping integral between the Wannier orbitals give information about energy scales in the system. This information can be useful in the formulation of a “simple” tight binding model necessary for a realistic description of CeRh_2As_2 system.

The model parameters are presented schematically in Fig. 7. Here, we introduced a distinction between atoms depending on their location in the crystal. For the structure presented in Fig 1(a), we get: Ce(1)-Rh(2)-As(1)-Rh(2)-Ce(2)-As(2)-Rh(1)-As(2)-Ce(1) going from the top to the bottom. As one can see, As(1) and Rh(1) atoms form the square lattice and they are located be-

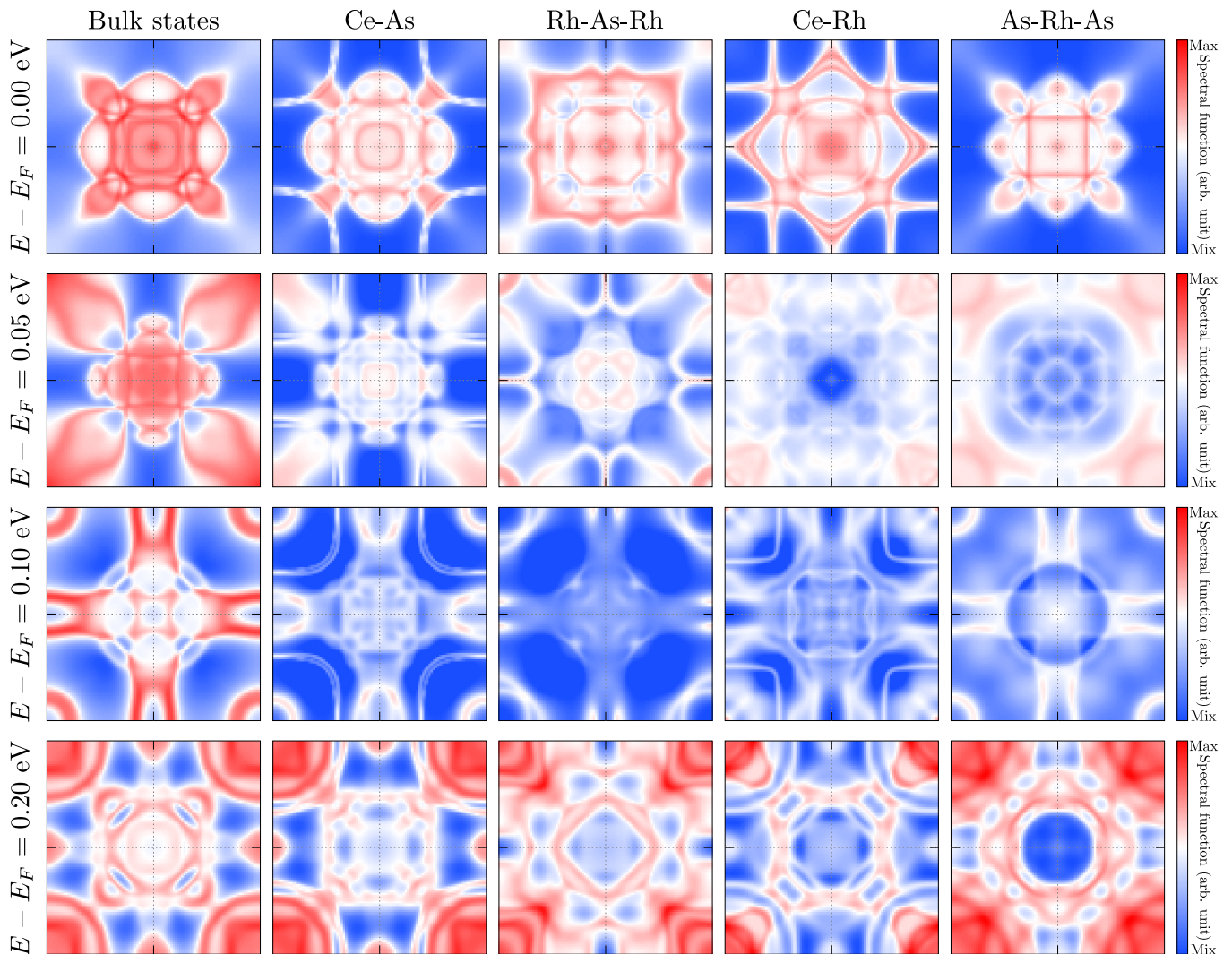


FIG. 6. The Fermi surface and constant energy contours (from the top to the bottom, for energies above the Fermi level as given). Panels from left to right present results for bulk states or surface states with specified surface termination (as labeled).

tween Rh(2) and As(2) atoms, respectively.

Let us start the discussion from the onsite energies [Fig. 7(a)]. In the case of Ce atoms, the d and f orbitals have comparable onsite energy of 1.32 eV above the Fermi level. The CEF mostly does not depend on the position and is around 1–50 meV for d orbitals or 10–145 meV for f orbitals. The spin-orbit interaction introduces additional onsite energy splitting in range of 10–20 meV for d orbitals, and 6–28 meV for f orbitals. Next, the d orbitals of Rh atoms are located around energy -2 eV. Difference between onsite energy of Rh(1) and Rh(2) orbitals is around 80 meV. In the case of Rh(1) atoms, the CEF is around 9–165 meV, while the SOC splitting is around 1–40 meV. Contrary to this, for Rh(2) atoms, the CEF is around 58–630 meV, whereas the SOC splitting is found around 2–5 meV. Finally, the p orbitals of As atoms are located around energy -1.6 eV for As(1) and -2.18 eV for As(2). In this case, the difference for the onsite ener-

gies for As atoms is the biggest and shows how important their environments are. What is surprising, the CEF for both As atoms are comparable, within range 15–45 meV. The SOC splitting is much stronger in the case of As(1) atoms (around 30 meV), while for As(2) atoms is mostly unnoticeable (smaller than 2 meV). Estimated here CEF is much larger than suggested earlier [11], what indicates higher Kondo temperature.

The absolute values of the hopping integrals between the Wannier orbitals are presented in Fig. 7(b). Every dot corresponds to the hopping integrals between specified orbitals, while a size of dot corresponds to the magnitude of the hopping. The parameters are divided into blocks describing hoppings (given as overlapping) between specified atomic orbitals (as labeled from the left and from the top in the figure). The diagonal block (with the yellow background) corresponds to hoppings between orbitals of the same type of atoms (typically

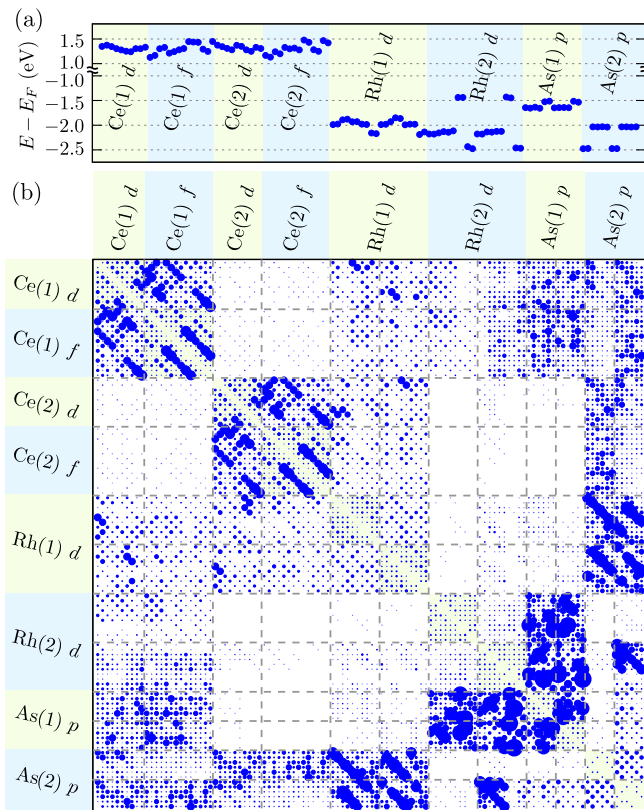


FIG. 7. Comparison of (a) the Wannier orbitals onsite energies and (b) absolute values of the hopping integrals between Wannier orbitals (represented by the dot sizes).

intraorbital hoppings between different orbitals). Similarly, non-diagonal blocks correspond to the hopping between orbitals centered on different atoms. What is interesting, the interatomic hopping between some atoms (e.g., As(1) and Rh(2) or As(1) within As square net) are bigger than the intraorbital hoppings. In the diagonal blocks, only hoppings between some d orbitals or some f orbitals of Ce are noticeably big (e.g., first four diagonal blocks). It is noticeable that the hoppings between the orbitals of atoms creating RhAs-layers are dominating in the system [i.e. Rh(1) and As(2) or As(1) and Rh(2) atoms]. Similarly, inter-atomic hoppings within the square nets are noticeably large [hoppings between Rh(1) orbitals or As(1) orbitals]. What is more, the hoppings between Ce(1) and Ce(2) atoms are negligible small, what can be related to the relatively large distance between these atoms or screening of the atoms by the RhAs-layers. Moreover, one should notice that the hoppings between Ce atoms and other atoms exhibit strong dependence on the relative position. For Ce(1) atoms, the hoppings to all Rh and As atoms are significant, while for Ce(2) atoms only hopping to Rh(1) and As(2) atoms is noticeably large. In practice, hoppings between from Ce(2) to As(1) and Rh(2) are smaller than 1 meV.

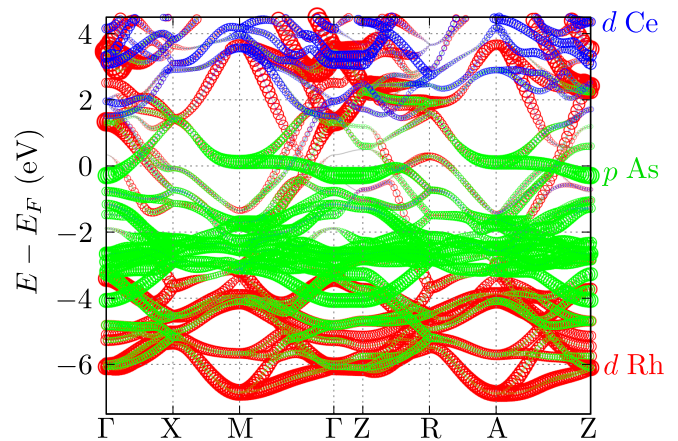


FIG. 8. The electronic band structure of CeRh_2As_2 projected on selected orbitals. The results for f states treated as a core states. Colors of the dots correspond to types of the orbitals, while size of the dots are associated with their contribution strength. Red, green, and blue colors correspond to d Rh, p As, and d Ce orbitals, respectively.

IV. SUMMARY

In this paper, we analyzed the electronic band structure of CeRh_2As_2 compound. We compared the results for this materials with findings for LaRh_2As_2 . In the case of the Ce f electrons treated as a core states, the electronic band structures are similar for both materials. The Fermi surface also reflect this similarity. Contrary to this, for the Ce f electrons treated as a valence states, the electronic band structure is more complex above the Fermi surface. The f states are well visible in a form of nearly-flat bands well-hybridized with other states [4]. Such complex structure and close vicinity of the Ce f states to the Fermi level have important role on the obtained results.

Strong sensitivity of the electronic band structure is well visible in the recently presented ARPES spectra [17, 18]. In one of them, the Ce f flat states are visible below the Fermi level. Nevertheless, our study of the slab-like calculation within the surface Green's function method reproduces the observed experimental spectra well. Depending on the surface termination, the system can realized the surface states visible in the spectral function, what can give information about termination realized experimentally. Our results clearly reproduce the experimentally observed Fermi surface. This can suggest a smaller role of the correlation on the electronic band structure then expected.

The recently developed model of CeRh_2As_2 is formulated from the Ce-sites perspective [14, 15]. However, performing analyses of the tight binding models based on the maximally localized Wannier orbitals from direct electronic band structure calculations give several interesting information about CeRh_2As_2 electronic energy scales. First, the observed crystal fields are big-

ger then reported previously [11]. Second, the Ce atoms play nonequivalent role in the energetic scale of the system. Here, the hopping between Ce atoms is negligible small with respect to other hoppings. Our analyses uncover strong hybridization within the Rh-As layers. This opens a new question about more adequate models of CeRh_2As_2 describing also the role of As-Rh layers. Finally, we would like point that the CeRh_2As_2 exhibits several similar properties like simple iron-based superconductor FeSe [8] (both with $P4/nmm$ symmetry). In the case of iron-based superconductors, the iron-arsenide or iron-selenide layers play important role on the physical properties. Similarly, for CeRh_2As_2 , it can be atomic layers formed by As and Rh atoms. This can be also supported by the exact analyses of the electronic band structure obtained from DFT calculations [4]. In the case of CeRh_2As_2 , the bands crossing the Fermi level are mostly related with As p and Rh d orbitals (see Fig. 8). As a

result, the role of the As-Rh layer (and square-like lattice of As and Rh atoms) can play more important role on the physical properties of CeRh_2As_2 than initially assumed. The properties of these layers should be more carefully studied in the future theoretical and experimental investigations.

ACKNOWLEDGMENTS

We kindly thank Daniel F. Agterberg and Aline Ramires for helpful comments and insightful discussions. Some figures in this work were rendered using VESTA [33] and XCRYSDEN [34] software. A.P. is grateful to Laboratoire de Physique des Solides in Orsay (CNRS, University Paris Saclay) for hospitality during a part of the work on this project. A.P. kindly acknowledges the support by the National Science Centre (NCN, Poland) under Project No. 2021/43/B/ST3/02166.

-
- [1] S. Khim, J. F. Landaeta, J. Banda, N. Bannor, M. Brando, P. M. R. Brydon, D. Hafner, R. K uchler, R. Cardoso-Gil, U. Stockert, A. P. Mackenzie, D. F. Agterberg, C. Geibel, and E. Hassinger, Field-induced transition within the superconducting state of CeRh_2As_2 , *Science* **373**, 1012 (2021).
- [2] H. Siddiquee, Z. Rehfuss, C. Broyles, and S. Ran, Tuning the parity of superconductivity in CeRh_2As_2 via pressure (2022), [arXiv:2212.06930](https://arxiv.org/abs/2212.06930).
- [3] S. Kitagawa, M. Kibune, K. Kinjo, M. Manago, T. Taniguchi, K. Ishida, M. Brando, E. Hassinger, C. Geibel, and S. Khim, Two-dimensional XY-type magnetic properties of locally noncentrosymmetric superconductor CeRh_2As_2 , *J. Phys. Soc. Jpn.* **91**, 043702 (2022).
- [4] A. Ptok, K. J. Kapcia, P. T. Jochym, J. La zewski, A. M. Ole s, and P. Piekarczyk, Electronic and dynamical properties of CeRh_2As_2 : Role of Rh_2As_2 layers and expected orbital order, *Phys. Rev. B* **104**, L041109 (2021).
- [5] M. Kibune, S. Kitagawa, K. Kinjo, S. Ogata, M. Manago, T. Taniguchi, K. Ishida, M. Brando, E. Hassinger, H. Rosner, C. Geibel, and S. Khim, Observation of antiferromagnetic order as odd-parity multipoles inside the superconducting phase in CeRh_2As_2 , *Phys. Rev. Lett.* **128**, 057002 (2022).
- [6] S. Ogata, S. Kitagawa, K. Kinjo, K. Ishida, M. Brando, E. Hassinger, C. Geibel, and S. Khim, Parity transition of spin-singlet superconductivity using sublattice degrees of freedom, *Phys. Rev. Lett.* **130**, 166001 (2023).
- [7] J. F. Landaeta, P. Khanenko, D. C. Cavanagh, C. Geibel, S. Khim, S. Mishra, I. Sheikin, P. M. R. Brydon, D. F. Agterberg, M. Brando, and E. Hassinger, Field-angle dependence reveals odd-parity superconductivity in CeRh_2As_2 , *Phys. Rev. X* **12**, 031001 (2022).
- [8] D. C. Cavanagh, T. Shishidou, M. Weinert, P. M. R. Brydon, and D. F. Agterberg, Nonsymmorphic symmetry and field-driven odd-parity pairing in CeRh_2As_2 , *Phys. Rev. B* **105**, L020505 (2022).
- [9] A. Ptok, K. J. Kapcia, A. Cichy, A. M. Ole s, and P. Piekarczyk, Magnetic Lifshitz transition and its consequences in multi-band iron-based superconductors, *Sci. Rep.* **7**, 41979 (2017).
- [10] K. Machida, Violation of Pauli-Clogston limit in the heavy-fermion superconductor CeRh_2As_2 : Duality of itinerant and localized $4f$ electrons, *Phys. Rev. B* **106**, 184509 (2022).
- [11] D. Hafner, P. Khanenko, E.-O. Eljaouhari, R. K uchler, J. Banda, N. Bannor, T. L uhmann, J. F. Landaeta, S. Mishra, I. Sheikin, E. Hassinger, S. Khim, C. Geibel, G. Zwicky, and M. Brando, Possible quadrupole density wave in the superconducting kondo lattice CeRh_2As_2 , *Phys. Rev. X* **12**, 011023 (2022).
- [12] D. S. Christovam, M. Ferreira-Carvalho, A. Marino, M. Sundermann, D. Takegami, A. Melendez-Sans, K. D. Tsuei, Z. Hu, S. Roessler, M. Valvidares, M. W. Haverkort, Y. Liu, E. D. Bauer, L. H. Tjeng, G. Zwicky, and A. Severing, Spectroscopic evidence of kondo-induced quasi-quartet in CeRh_2As_2 (2023), [arXiv:2308.10663](https://arxiv.org/abs/2308.10663).
- [13] T. Hazra and P. Coleman, Triplet pairing mechanisms from Hund's-Kondo models: Applications to UTe_2 and CeRh_2As_2 , *Phys. Rev. Lett.* **130**, 136002 (2023).
- [14] D. M ockli and A. Ramires, Two scenarios for superconductivity in CeRh_2As_2 , *Phys. Rev. Res.* **3**, 023204 (2021).
- [15] D. M ockli and A. Ramires, Superconductivity in disordered locally noncentrosymmetric materials: An application to CeRh_2As_2 , *Phys. Rev. B* **104**, 134517 (2021).
- [16] K. Nogaki, A. Daido, J. Ishizuka, and Y. Yanase, Topological crystalline superconductivity in locally noncentrosymmetric CeRh_2As_2 , *Phys. Rev. Res.* **3**, L032071 (2021).
- [17] Y. Wu, Y. Zhang, S. Ju, Y. Hu, G. Yang, H. Zheng, Y. Huang, Y. Zhang, H. Zhang, B. Song, N. C. Plumb, F. Steglich, M. Shi, G. Zwicky, C. Cao, H. Yuan, and Y. Liu, Quasi-two-dimensional Fermi surface and heavy quasiparticles in CeRh_2As_2 (2023), [arXiv:2309.06732](https://arxiv.org/abs/2309.06732).
- [18] X. Chen, L. Wang, J. Ishizuka, K. Nogaki, Y. Cheng, F. Yang, R. Zhang, Z. Chen, F. Zhu, Y. Yanase, B. Lv, and Y. Huang, Coexistence of near- E_F flat band and van

- Hove singularity in a two-phase superconductor (2023), [arXiv:2309.05895](https://arxiv.org/abs/2309.05895).
- [19] P. E. Blöchl, Projector augmented-wave method, *Phys. Rev. B* **50**, 17953 (1994).
- [20] G. Kresse and J. Hafner, Ab initio molecular-dynamics simulation of the liquid-metal–amorphous-semiconductor transition in germanium, *Phys. Rev. B* **49**, 14251 (1994).
- [21] G. Kresse and J. Furthmüller, Efficient iterative schemes for ab initio total-energy calculations using a plane-wave basis set, *Phys. Rev. B* **54**, 11169 (1996).
- [22] G. Kresse and D. Joubert, From ultrasoft pseudopotentials to the projector augmented-wave method, *Phys. Rev. B* **59**, 1758 (1999).
- [23] J. P. Perdew, A. Ruzsinszky, G. I. Csonka, O. A. Vydrov, G. E. Scuseria, L. A. Constantin, X. Zhou, and K. Burke, Restoring the density-gradient expansion for exchange in solids and surfaces, *Phys. Rev. Lett.* **100**, 136406 (2008).
- [24] H. J. Monkhorst and J. D. Pack, Special points for Brillouin-zone integrations, *Phys. Rev. B* **13**, 5188 (1976).
- [25] N. Marzari and D. Vanderbilt, Maximally localized generalized Wannier functions for composite energy bands, *Phys. Rev. B* **56**, 12847 (1997).
- [26] I. Souza, N. Marzari, and D. Vanderbilt, Maximally localized Wannier functions for entangled energy bands, *Phys. Rev. B* **65**, 035109 (2001).
- [27] N. Marzari, A. A. Mostofi, J. R. Yates, I. Souza, and D. Vanderbilt, Maximally localized wannier functions: Theory and applications, *Rev. Mod. Phys.* **84**, 1419 (2012).
- [28] G. Pizzi, V. Vitale, R. Arita, S. Blügel, F. Freimuth, G. Géranton, M. Gibertini, D. Gresch, C. Johnson, T. Koretsune, J. Ibañez-Azpiroz, H. Lee, J.-M. Lihm, D. Marchand, A. Marrazzo, Y. Mokrousov, J. I. Mustafa, Y. Nohara, Y. Nomura, L. Paulatto, S. Poncé, T. Ponweiser, J. Qiao, F. Thöle, S. S. Tsirkin, M. Wierzbowska, N. Marzari, D. Vanderbilt, I. Souza, A. A. Mostofi, and J. R. Yates, WANNIER90 as a community code: new features and applications, *J. Phys.: Condens. Matter* **32**, 165902 (2020).
- [29] M. P. L. Sancho, J. M. L. Sancho, J. M. L. Sancho, and J. Rubio, Highly convergent schemes for the calculation of bulk and surface Green functions, *J. Phys. F: Met. Phys.* **15**, 851 (1985).
- [30] Q. S. Wu, S. N. Zhang, H.-F. Song, M. Troyer, and A. A. Soluyanov, WANNIERTOOLS: An open-source software package for novel topological materials, *Comput. Phys. Commun.* **224**, 405 (2018).
- [31] S.-i. Kimura, J. Sichelschmidt, and S. Khim, Optical study of the electronic structure of locally noncentrosymmetric CeRh₂As₂, *Phys. Rev. B* **104**, 245116 (2021).
- [32] H. Li, H.-T. Ma, P.-F. Tian, D.-L. Guo, Y. Liu, X. Ming, and X.-J. Zheng, Phase evolution of ce-based heavy-fermion superconductors under pressure: a combined DFT+DMFT and effective-model description (2023), [arXiv:2310.06443](https://arxiv.org/abs/2310.06443).
- [33] K. Momma and F. Izumi, VESTA3 for three-dimensional visualization of crystal, volumetric and morphology data, *J. Appl. Crystallogr.* **44**, 1272 (2011).
- [34] A. Kokalj, XCRYSDEN—a new program for displaying crystalline structures and electron densities, *J. Mol. Graph. Model.* **17**, 176 (1999).